Integrating Pd-Doped Perovskite Catalysts with Ceramic Hollow Fibre Substrate for Efficient CO Oxidation

Nur Izwanne Mahyon [a,b], Tao Li [a], Billy Digjaya Tantra [a], Ricardo Martinez-Botas [c], Zhentao Wu [*d], Kang Li [*a]

[a] Barrer Centre, Department of Chemical Engineering, Imperial College London, South Kensington Campus, London, SW7 2AZ, United Kingdom

[b] UTM-Centre for Low Carbon Transport in cooperation with Imperial College London (UTM-LoCARtic), Universiti Teknologi Malaysia, 81310 Johor Bahru, Johor, Malaysia

[c] Department of Mechanical Engineering, Imperial College London, South Kensington Campus, London, SW7 2AZ, United Kingdom

[d] Aston Institute of Materials Research, School of Engineering and Applied Science, Aston University, Birmingham, B4 7ET, UK

* Corresponding Authors:

Dr. Zhentao Wu, z.wu7@aston.ac.uk; +44 (0)12 1204 3353

Prof. Kang Li, kang.li@imperial.ac.uk; +44 (0)20 7594 5676

Abstract

Doping Pd into perovskite catalysts helps to reduce light-off temperatures, improve thermal-chemical stability and lowered catalyst cost by decreasing Platinum Group Metals (PGMs). In this study, $LaFe_{0.7}Mn_{0.225}Pd_{0.075}O_3$ (LFMPO) and $LaFe_{0.7}Co_{0.225}Pd_{0.075}O_3$ (LFCPO) were synthesised, characterized and evaluated for catalytic treatment of automotive emissions, using CO oxidation as the model reaction. Such catalysts were further incorporated inside micro-structured ceramic hollow fibre substrates, and compared with a packed bed configuration by light-off temperatures. Performance evaluations suggest that, LFMPO deposited inside the hollow fibre substrate could be light up at 232 ^{o}C, which is 10 ^{o}C lower than a packed-bed counterpart with the same amount of catalyst (5 mg) and GHSV of ~5300 h^{-1}. While excessive incorporation of the catalyst (10 mg) generates significantly higher transfer resistance, which impairs catalytic performance of hollow fibre reactors, with CO conversion per gram of catalyst reduced from 0.01 mole g^{-1} to 0.0051 mole g^{-1}.

Keywords: Catalytic Converter, Ceramic Hollow Fibre, Perovskite Catalyst, Palladium, CO Oxidation, Light-off Temperature

Graphical Abstract

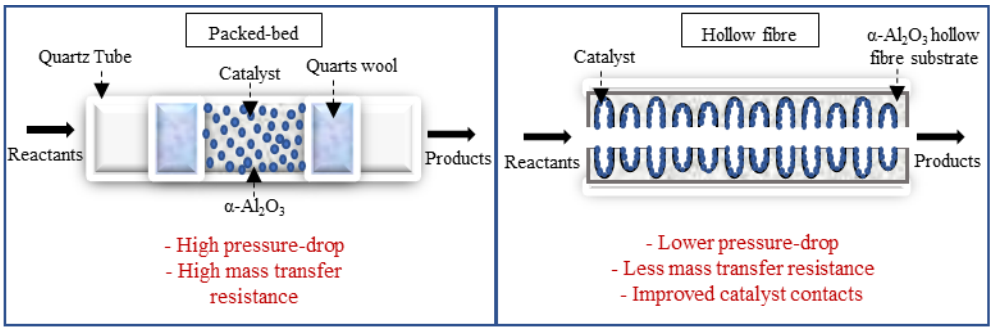

1. Introduction

Noxious gases such as carbon monoxide (CO), nitrogen oxides (NOx), and hydrocarbons (HCs) can be released from internal combustion engines due to incomplete combustion, which needs to be thoroughly treated for compliance with regulatory standards established [1]. As a common and efficient practice, exhaust systems involve catalytic converters as a core component, which enable catalytically conversion of noxious emissions into non-harmful species. Catalytic converters normally consist of three essential components: i) a monolithic substrate, ii) a washcoat layer with a high surface area, and iii) catalytic active metals, conventionally Platinum Group Metals (PGM) catalysts. Despite of significantly successful application of this technology, exhaust gases from gasoline combustion engines can reach temperatures of up to 1000 ^{o}C, leading to severe sintering of washcoat oxide, γ-Al_2O_3 [2], due to irreversible phase transition from γ-Al_2O_3 to α-Al_2O_3 under elevated temperatures. This significantly reduces surface area of the washcoat layer in which metal catalysts are dispersed, and consequently reduce catalytic performance and efficiency of catalytic converters As a result, a highly thermally and chemically robust catalytic washcoat is always essential to good long-term performance of catalytic converters.

In addition to long-term stability, scarcity of PGMs and their price volatility belong to a second challenge of catalytic converter technology [3]. These challenges have also sparked a lot of research with the aim to reduce the dependability on PGMs, and to formulate supported PGM catalysts with better thermal stability. Among the various catalyst technologies available for substituting PGMs, perovskite catalysts are attracting more and more research interest, due to the unique regenerative properties of perovskites reported in letters to Nature regarding their potential applications in exhaust treatment [4]. Other attractive characteristics of perovskite

catalysts include good flexibility and adaptability in their composition, thermal stability, abundant availability, and most importantly, much lower costs than PGMs, which also enables the use of this type of material for numerous applications other than exhaust treatment [5,6]. And similar to other reactions, the highly defective perovskite structure enables rapid exchange between oxygen atoms from surface carbonate and perovskite lattice oxygen, which enables efficient CO oxidation although detailed mechanism can be subject to chemical compositions of perovskites. A typical perovskite structure follows a ABO_3 formulation, with a large cation at a 12 coordinated A site, 6 smaller cations in the B site and an anion, most often oxygen [7]. In order to tailor the properties of a perovskite oxide, the A site and B site can be substituted by various elements. However, B site substitution normally has a more significant impact on the material properties, such as catalytic activity, and affects oxygen vacancy, which is important in altering the other properties of perovskites [8–11]. Till date, out of the many options of transition-based metal perovskites, lanthanum based perovskites have shown higher reactivity for an oxidation process, when coupled with Co, Mn, Fe, Cr or Ni in their B sites [12].

Tanaka et al. investigated regeneration ability of a perovskite, which responded in accordance with environmental input [13,14]. This enables the perovskite framework to accommodate metals that can also migrate from one site to another [4,15–18]. For example, the status of Pd inside the lattices of a perovskite changes reversibly between oxidation and reduction atmospheres, which benefits its long-term catalytic performance for exhaust treatment [10]. Such a change in the status of Pd suppresses the growth of Pd particles, which is usually caused by the sintering effects of conventional catalysts such as Pd/γ-alumina. As a result, doping Pd into perovskite will improve the long-term stability of the catalysts, while also using much lesser amounts of PGMs than conventional catalysts for exhaust treatment. Although

perovskites without PGMs are catalytic active to CO oxidation, the doping of Pd can effectively reduce light-off temperatures (Table 1). This is mainly due to increased concentration of oxygen vacancy which facilitates oxygen transport from catalyst bulk to surface [19–23]. Moreover, perovskite is subject to sulphur poisoning [24], which can be effectively delayed by doping Pd [25].

Despite aforementioned advantages of perovskite catalysts, their specific surface area is normally much smaller than conventional washcoat materials. This creates challenges in the potential applications of perovskites, since a larger amount of such catalysts have to be used in order to compensate for the high surface area required for a sufficiently good reaction efficiency. To address a challenge of this nature, a more advanced substrate enabling intensified interactions between the catalyst and reactants is necessary. In one of our previous studies, the potential of using a micro-structured ceramic hollow fibre substrate for a new catalytic converter design has been proved [26]. This new design offers a greater accessible surface area that originates from the unique microchannel structure inside the substrate, which also facilitates the deposition of different catalysts. Intensified transfer processes inside such substrates significantly increase catalyst utilisation, which is key to addressing the low specific surface area of perovskite catalysts. As a second benefit of depositing perovskite catalyst into such substrates, conventional washcoating materials are not needed, which ease the issue of sintering of washcoat layers, a main reason of the reduced performance of a conventional catalytic converter.

In this study, two different types of perovskites, $LaFe_{0.7}Mn_{0.225}Pd_{0.075}O_3$ (LFMPO) and $LaFe_{0.7}Co_{0.225}Pd_{0.075}O_3$ (LFCPO) were synthesised using a sol-gel method via citrate complexation. These perovskite catalysts were deposited inside a hollow fibre substrate, with

no washcoat materials, for catalytic conversion of CO, and compared with conventional packed bed reactor. This study presents research, conducted for the first time, into the incorporation of a perovskite catalyst without any washcoat layer, into a hollow fibre substrate for catalytic converter applications. Effects of catalyst packing inside hollow fibre substrates on CO oxidation was also outlined.

2. Experimental

2.1 Materials

Lanthanum (III) nitrate hydrate 99.9% trace metals basis, iron (III) nitrate nonahydrate, ≥ 99.95% trace metals basis, manganese (II) nitrate hydrate 98%, cobalt (III) nitrate hexahydrate, and palladium (II) chloride 99.999% were purchased from Sigma-Aldrich. Hydrochloric acid 37% vol%, ethanol absolute, AnalaR NORMAPUR, Assay (V/V) 99.95%, and ethylene glycol (Assay on anhydrous substance min. 98% and citric acid anhydrous (ACS Reagent ≥ 99.5%) were purchased from VWR. γ-Alumina powder (Al_2O_3) with a surface area of 100 ± 30 m^2 g^{-1} and α-alumina (Al_2O_3) powder (1 μm, 99.9% metal basis, surface area 6 –8 m^2 g^{-1}) were purchased from Inframat Advance Materials. All chemicals were used as supplied.

2.2 Catalyst Preparation

Two perovskite oxide catalysts, $LaFe_{0.7}Mn_{0.225}Pd_{0.075}O_3$ (LFMPO) and $LaFe_{0.7}Co_{0.225}Pd_{0.075}O_3$ (LFCPO), were synthesised by a sol-gel method via citrate complexation (Figure 1). Stoichiometric amounts of lanthanum, iron, manganese or cobalt nitrate were dissolved in a solution of de-ionised water (5 ml) and ethanol (15 ml). The stoichiometric ratio was calculated

on the basis of 4 mmol of lanthanum. The mixture obtained was treated in an ultrasonic bath for 15 minutes, to ensure uniform mixing of the chemicals.

Meanwhile, palladium (II) chloride was added into a hydrochloric acid solution (0.05 M) at a molar ratio of 1:1.5($PdCl_2$:HCl), which was heated at 80 ^oC for 30 minutes until a clear solution was obtained. It was then mixed with the metal nitrate solution and further treated in an ultrasonic bath for 30 minutes. Subsequently, an aqueous solution containing excessive citric acid (115% of the total moles of metal cations) was added, which enabled the complexation of metal cations after being stirred for one hour. The mixture obtained was continuously stirred and treated at 80 ^oC overnight to obtain the precursor powder, prior to a second drying at 80 ^oC for eight hours to remove remaining moisture. The precursor powder was then calcined at 700 ^oC for four hours, as shown in Figure 1. The catalyst obtained was then ground into fine particles for characterizations and tests.

Meanwhile, catalysts consisting of 0.075 wt.% palladium supported on γ-Al_2O_3 were prepared by a wet incipient impregnation method. In a general process, a palladium chloride solution was mixed with γ-Alumina powder, stirred for one hour, dried overnight at 120 ^oC, and calcined for one hour at 500 ^oC, or 700 ^oC for four hours to obtain the catalysts.

2.3 Incorporation of Perovskite Catalysts into Hollow Fibre Substrates

Incorporation of catalysts into alumina hollow fibre substrates, which were prepared through a phase-inversion assisted extrusion process, has been described in our previous work [26]. For preparation of a hollow fibre substrate, a uniform slurry consisting of poly(methyl methacrylate) (PMMA) binder, N-Methyl-2-pyrrolidone (NMP) solvent, Arlacel P135

dispersant, and α-Al_2O_3 powder was prepared. It was then extruded through a spinneret, together with a second stream of internal coagulant, into an external water bath to form the precursor hollow fibre substrates. The precursor hollow fibre was then straightened, dried at room temperature, cut, and finally sintered at 1500 ˚C to obtain the alumina hollow fibre substrates. Incorporation of catalysts into hollow fibre substrate has been described in Supplementary Information of our earlier work [26]**.** In general, 50 mg of perovskite catalyst was first dispersed inside 500 ml of distilled water (ultrasonic bath for one hour). The mixture was then pumped through hollow fibre substrates with pre-determined length for a certain period of time, and dried at 150 °C for one hour. Weight increment due to catalyst deposition was measured and recorded, before a second cycle of catalyst incorporation. This process was repeated until the target loadings of perovskite catalyst were obtained. No extra secondary oxide / washcoat layer was used in this study.

2.4 Characterisation

A morphology evaluation of hollow fibre substrates was carried out at different magnifications using a JOEL JSM-5610 scanning electron microscopy (SEM). Brunauer-Emmett-Teller (BET) was used to investigate the surface area of catalysts and catalyst/hollow fibre composite, and performed via a Micromeritics TRISTAR Surface area analyser using N_2 as the non-corrosive gas. Prior to the analysis, samples were dried overnight at 110 ^{o}C. A porometer (Porolux 100) and gas permeation tests (hollow fibre samples of 25 mm long) were used to investigate the effect of the catalyst deposition on the transport process of CO oxidation. Phase composition of the perovskite catalysts were analysed via a PANalytical X-ray diffractometer (XRD). Crystallite size was calculated by using the Scherrer equation below:

$$D = \frac{K\lambda}{\beta \cos \theta} \qquad \text{(Eq. 1)}$$

Where D = the average thickness in a vertical direction of the crystal face, K is Scherrer constant, λ is the wavelength of X-ray, β is the half high width of the diffraction peak of the sample, θ is the Bragg diffraction angle.

2.5 Performance evaluation – CO oxidation

CO oxidation was used to evaluate the catalytic performance of the perovskite catalysts and the perovskite/hollow fibre structured composite, which also facilitated the comparison with our earlier work which involved Pd/γ-alumina as the catalyst. Two different catalyst packing configurations were chosen (Figure 2). For the packed-bed configuration, 5 mg of perovskite catalyst (average particle size of 5 μm) was mixed with 200 mg of α-Al_2O_3 powder (particle size of ~ 1 μm), before being loaded into a quartz tube and secured by quartz wool at both ends of the catalyst bed. The catalyst bed was approximately 20 mm in length. For the structured configuration, 5 ± 0.5 mg of catalyst was deposited into alumina hollow fibre of 50 mm long, which weighed at approximately 200 ± 10 mg. The hollow fibre sample was mounted into the quartz tube connected to a metal coil to pre-heat the gaseous reactants to the reaction temperature. The quartz tube was placed horizontally in a furnace (Vecstar Furnace, VCTF/SP). Mass flow controllers (Model 0154, Brooks Instrument) were used to control the gas flow into the system. A mixture of air and CO (10% CO in 90% Argon) at a ratio of 1:1 was fed into the reactor system, which represents the lean-burn condition with an excess of oxygen. The flow rate of the feed gas was calculated to achieve a space velocity GHSV of ~ 5300 h^{-1}. An on-line gas chromatograph (Varian 3900) was connected to the outlet stream to analyse the effluent. The reaction temperature was gradually increased, and the sampling was

taken after thirty minutes of temperature stabilisation intervals. A series of reaction temperatures were used, from room temperature until 100% of the CO conversion. The conversion of CO was calculated based on the equation below (Eq. 2)

$$\% \text{ conversion of CO} = \frac{C_{CO\ inlet} - C_{CO\ outlet}}{C_{CO\ inlet}} \times 100\% \qquad \text{(Eq. 2)}$$

Where $C_{CO\ inlet}$ and $C_{CO\ outlet}$ are the CO concentrations at the inlet and outlet of the system, respectively. The details of the reaction test set up has been described in our previous study [26].

3. Results and Discussion

3.1 Phase composition of perovskite catalysts

Figure 3 shows the XRD pattern of the LFMPO and LFCPO, which were calcined at 700 ^{o}C for four hours and have an orthorhombic crystal structure. The XRD patterns also indicate that a calcination temperature of 700 ^{o}C can enable good transformation of the synthesised perovskites [27]. Further reducing the calcination temperature helps to reduce grain size of perovskites, which can benefit catalytic reactions by providing larger catalytic areas. However, phase segregation can occur at 660 ^{o}C [28], which changes catalyst composition and impairs catalytic performance as a consequence. As a result, 700 ^{o}C was used for calcination of LFMPO and LFCPO in this study.

The XRD patterns in Figure 3 indicate that there is a small peak at the 2θ value of 33°, which is next to the main perovskite peak of LFMPO and LFCPO. This small peak indicates the presence of PdO [29], as a result of incomplete integration of Pd into perovskite oxides. If a calcination temperature higher than 700 °C was used, a full integration of Pd can be possible [29]. However, it should be noted that full integration of Pd into perovskite lattices may retard catalytic performance, compared to Pd supported on perovskites which is more active due to easier interactions with reactants [30,31] . In contrast to washcoat materials such as γ-Al_2O_3, perovskites are thermally more robust. Integrating Pd with perovskite is thus expected to have less problems of catalyst sintering as γ-Al_2O_3, benefiting life-time of catalysts.

As a common washcoat material with high surface area, γ-Al_2O_3 is well-known for its microstructural evolution when exposed to high temperatures. This is due to phase transitions from γ to the meta-stable δ-θ, and finally thermodynamically-stable α phase, which results in the densification of washcoat layers, reduction in the specific surface area and consequently in deteriorating catalytic performance. For example, 5mg of 0.075 Pd/ γ-Al_2O_3 synthesised at 500 °C was deposited inside ceramic hollow fibre substrates, which increased BET surface area of the composite, as shown in Table 2. While after thermal treatment at 700 °C, a reduction of 12.3 % in specific surface area can be observed. Here, the cations and anions in the γ-Al_2O_3 undergo rearrangement until they reach a dense corundum structure where the rearrangements result in the loss of support surface area [32]. In contrast, perovskite catalysts with fully a developed phase structure (Table 1) have no such problems. But due to the low specific surface area (Table 2) and potential reactions between perovskites and γ-Al_2O_3 that impairs catalytic performance [33,34], perovskite catalysts are deposited inside hollow fibre substrates made of α-alumina and with a unique bi-modal pore structure in this study.

3.2 Micro-structure of perovskites/hollow fibre substrate

Figure 4 (a) presents a cross-section of the hollow fibre substrate with a bi-modal pore structure [35], which consists of packed-pores of approximately 200 nm and many oriented microchannels for which perovskite catalysts were deposited. LFMPO (Figure 4 (b)) and LFCPO (Figure 4 (c)) catalysts were deposited on the micro-channels and show an average particle size of approximately 5 μm, which is much larger than the α-alumina used for preparing the hollow fibre substrates.

Morphologies of hollow fibre substrates deposited with 5 ± 0.5 mg of perovskite catalysts are displayed in Figure 5. As seen in a(i) and a(ii), hollow fibre substrates have open microchannel ends at the inner surface that is approximately 40 μm in diameter. Substrates of this type could provide a GSA value of approximately 40.7 cm^2cm^{-3}, which is the same as that of a conventional monolith of 750 CPSI (GSA of 40.2 cm^2cm^{-3}) [26]. A deposition of 5 ± 0.5 mg of perovskite catalysts maintains good microchannel openings at both the inner surface and cross-section, as shown in Figure 5(b(i), b(ii), c(i) and c(ii)), by forming a thin catalyst layer along the surface of the microchannels. This is critical to the efficient interaction between the gaseous reactants and catalysts deposited inside the hollow fibre substrate [36].

By increasing the amount of perovskite catalysts to approximately 10 mg, catalyst particles start to form mini-packed-beds inside the microchannel of hollow fibre substrates. As can be seen in Figure 6, approximately 50% of the microchannel volume is filled by the LFMPO catalyst, with the microchannel endings at the substrate's inner surface remaining open (a(i)

and a(ii)). In contrast, the microchannel is largely filled with the LFCPO catalyst, which also blocks the microchannel endings at the inner surface of the substrate (b(i) and b(ii)). An increasing amount of perovskite catalyst inside the hollow fibre substrates provides more active sites for the catalytic reaction to proceed, which is supposed to benefit the conversion of CO in this study. Meanwhile, the formation of mini-packed-beds (Figure 6) indicates a higher transfer resistance compared to the catalyst layer in Figure 5, which retards the access of CO to the active sites of perovskite catalysts and consequently reduces the efficiency of the reaction.

3.3 Evaluation of catalytic performance - CO oxidation

Two reactor configurations were employed in this study to investigate the catalytic performance of perovskite catalysts, which include a conventional packed-bed reactor as the benchmark of catalyst performance, and a second hollow fibre reactor which can potentially be developed into a new generation of catalytic converter for automotive emissions control, due to its structural advantages over ceramic monoliths reported in our earlier work [26].

3.3.1 Packed bed reactor

A packed-bed configuration is commonly used for investigating catalyst performance, due to an irregular flow through the voids of packing, where it creates a turbulent mixing at Reynolds numbers lower than conservative domains. This enhances the fluid transport through the braiding effect and increases contact with the catalyst through enhanced diffusion [37]. For the packed bed reactor in this study, 5 mg or 10 mg of perovskite catalysts were mixed with 200 mg of α-Al_2O_3 and packed inside a quartz tube reactor. Figure 7 represents the CO conversion as a function of operating temperatures, with the corresponding values of T_{50} (the light-off

317 temperature at 50% of CO conversion) listed in Table 3. As can be seen, LFMPO shows a
318 conversion of CO higher than LFCPO at temperatures over 200 ^{o}C, which is in line with the
319 higher surface area of LFMPO (Table 2). In addition, since the catalytic process can be altered
320 by modifying the interactions between the B-site species and the oxygenated species in the
321 perovskite lattice, the change in oxygen vacancy concentration alters the catalytic activity.
322 From a material point of view, Mn has a higher number of oxidation states than Co. This
323 contributes to a higher synergistic activity brought about by Mn substitution. By doubling the
324 amount of catalyst inside the packed-bed reactor, T_{50} of LFMPO reduces from 242 ^{o}C to 213
325 ^{o}C, with LFCPO reduced from 252 ^{o}C to 235 ^{o}C (Table 3), which is still higher than commercial
326 counterparts. However, the better thermal stability of perovskite catalysts would enable them
327 to be placed closer to the engine to maintain a good catalytic performance, although this is not
328 perfect to cold start.
329
330 **3.3.2 Packed bed reactor vs hollow fibre reactor**
331
332 For hollow fibre reactors, the reaction of CO oxidation was performed by maintaining the same
333 conditions as the packed bed reactors, in terms of the amount of perovskite catalyst and the
334 space velocity (GHSV of ~ 5300 h^{-1}). For hollow fibre reactors with 5 mg of perovskite
335 catalysts (Figure 8 and Table 4), LFMPO shows higher conversion of CO than LFCPO, and
336 this is in line with a packed bed reactor (Figure 7). Moreover, the hollow fibre reactor shows a
337 light-off temperature lower than that of the packed bed counterpart. For instance, the light-off
338 temperature of LFMPO shifted from 242 ^{o}C in packed-bed to 232 ^{o}C in the hollow fibre reactor
339 (Table 4).
340

In contrast to a packed-bed reactor, in which the reactants "flow through" the porous bed, a hollow fibre reactor has a very different flow pattern. Instead of "flowing through", the bulk of the reactants flow along the length of the direction of the hollow fibre substrate, relying on a much slower diffusion process in the radial direction, for accessing the catalyst that is deposited. As a result, the reduction in the light-off temperature is mainly due to the structural advantages of hollow fibre substrates, together with the formation of a thin catalyst layer along the microchannels inside the substrate (Figure 5). This enables better and more uniform access of the reactants to the perovskite catalysts deposited, with less transfer resistance and agreeing well with our previous studies [26].

By increasing the amount of catalyst to 10 mg, mini-packed-beds are formed inside the microchannels (Figure 6). It is interesting to see that hollow fibre reactors performed worse than packed bed counterparts (Figure 9 and Table 5). With the same amount of catalysts involved, the light-off temperatures increased from 215 ^{o}C of packed-bed to 222 ^{o}C of hollow fibre reactor for LFMPO, while the one for LFCPO increased from 237 ^{o}C to 245 ^{o}C (Table 5). By comparing the CO oxidation results in Figures 7 - 9, it is quite obvious, that the formation of the mini-packed-beds inside the microchannels significantly increase the diffusion resistance in the radial direction of the hollow fibre substrates, which reduces the efficiency of catalyst utilization and consequently increases the light-off temperature.

To further understand how transfer hindrance affects the conversion of CO, which relies on the format of perovskite catalyst packing inside the microchannels of the hollow fibre substrate, gas permeation tests were performed and the results illustrated in Figure 10. As can be seen, the permeation flux for the hollow fibre reactors with 5 mg catalysts is significantly higher than the one with 10 mg of catalysts. Furthermore, the permeation flux of LFMPO-10 mg is almost

double the one of LFCPO-10 mg, which agrees well with Figure 6 (a-ii) and (b-ii). This also indicates that, an excessive catalyst deposition does not work for the hollow fibre reactor design, since the actual catalyst involved in the reaction is reduced due to the significantly increased transfer resistance. In this study, for the hollow fibre reactor with 5 mg of perovskite catalysts, 0.01 mole of CO was oxidized per gram of catalyst involved. This value was reduced significantly to 0.0051 mole g^{-1} for the hollow fibre reactor with 10 mg of catalyst, representing a nearly 50% reduction in catalyst utilization.

4. Conclusions

$LaFe_{0.7}Mg_{0.225}Pd_{0.075}O_3$ and $LaFe_{0.7}Co_{0.225}Pd_{0.075}O_3$ with a orthorhombic structure were synthesised in this study. These catalysts were then deposited inside hollow fibre substrates for CO oxidation, the results of which were compared with packed-bed reactors. Results of CO oxidation suggests that incorporation of 5 mg LFMPO and LFCPO catalyst into the hollow fibre could be light-up at 232 ^oC and 248 ^oC, respectively, which is 3% lower than the packed-bed counterpart with the same amount of catalyst at GHSV of ~ 5300 h^{-1}. Further incorporation of a 10 mg catalyst inside the hollow fibre resulted in a lowered catalyst utilization, where the moles of CO converted per unit mass of catalyst reduced from 0.01 mole g^{-1} for 5mg catalyst to 0.0051 g^{-1} for the 10 mg catalyst. This is mainly due to the higher mass transfer resistance when micro-channels were filled with perovskite particles. As a result, a better approach of forming a thin catalytic layer along the surface of micro-channels will be the key to improving performance of catalytic hollow fibre investigated in this study.

Acknowledgements

The authors would like to acknowledge the research funding provided by EPSRC (EP/R029180/1) in the United Kingdom. Nur Izwanne Mahyon would like to extend her gratitude to the Minister of Higher Education, Malaysia and the Universiti Teknologi Malaysia for financing her studies bursaries.

References

[1] W. Martin, M. Ray, A technical summary of Euro 6/VI vehicle emission standards, ICCT Brief. Pap. (2016) 1–17. http://www.theicct.org/sites/default/files/publications/ICCT_Euro6-VI_briefing_jun2016.pdf.

[2] A.S. Ivanova, E.M. Slavinskaya, R. V. Gulyaev, V.I. Zaikovskii, O.A. Stonkus, I.G. Danilova, L.M. Plyasova, I.A. Polukhina, A.I. Boronin, Metal-support interactions in Pt/Al2O3and Pd/Al2O3catalysts for CO oxidation, Appl. Catal. B Environ. 97 (2010) 57–71. doi:10.1016/j.apcatb.2010.03.024.

[3] L. Zhang, I.A.W. Filot, Y.Q. Su, J.X. Liu, E.J.M. Hensen, Understanding the Impact of Defects on Catalytic CO Oxidation of LaFeO 3 -Supported Rh, Pd, and Pt Single-Atom Catalysts, J. Phys. Chem. C. 123 (2019) 7290–7298. doi:10.1021/acs.jpcc.9b01520.

[4] Y. Nishihata, J. Mizuki, T. Akao, H. Tanaka, M. Uenishi, M. Kimura, T. Okamoto, N. Hamada, Self-regeneration of a Pd-perovskite catalyst for automotive emissions control., Nature. 418 (2002) 164–167. doi:10.1038/nature00893.

[5] N. Labhasetwar, G. Saravanan, S. Kumar Megarajan, N. Manwar, R. Khobragade, P. Doggali, F. Grasset, Perovskite-type catalytic materials for environmental applications, Sci. Technol. Adv. Mater. 16 (2015) 36002. doi:10.1088/1468-6996/16/3/036002.

[6] E. Grabowska, Selected perovskite oxides: Characterization, preparation and photocatalytic properties-A review, Appl. Catal. B Environ. 186 (2016) 97–126. doi:10.1016/j.apcatb.2015.12.035.

[7] S. Vasala, M. Karppinen, A2B′B″O6 perovskites: A review, Prog. Solid State Chem. 43 (2015) 1–36. doi:10.1016/j.progsolidstchem.2014.08.001.

[8] J. Zhu, A. Thomas, Perovskite-type mixed oxides as catalytic material for NO removal, Appl. Catal. B Environ. 92 (2009) 225–233. doi:10.1016/j.apcatb.2009.08.008.

[9] C. Moure, O. Peña, Recent Advances in Perovskites: Processing and Properties, Prog. Solid State Chem. 43 (2015) 123–148. doi:10.1016/j.progsolidstchem.2015.09.001.

[10] J. Zhu, H. Li, L. Zhong, P. Xiao, X. Xu, X. Yang, Z. Zhao, J. Li, Perovskite Oxides: Preparation, Characterizations, and Applications in Heterogeneous Catalysis, (n.d.). doi:10.1021/cs500606g.

[11] H. Zhu, P. Zhang, S. Dai, Recent Advances of Lanthanum-Based Perovskite Oxides for Catalysis, ACS Catal. 5 (2015) 6370–6385. doi:10.1021/acscatal.5b01667.

[12] H. Ziaei-azad, A. Khodadadi, P. Esmaeilnejad-ahranjani, Y. Mortazavi, Effects of Pd on enhancement of oxidation activity of LaBO3 (B = Mn , Fe , Co and Ni) pervoskite catalysts for pollution abatement from natural gas fueled vehicles, Appl. Catal. B Environ. Environ. 102 (2011) 62–70. doi:10.1016/j.apcatb.2010.11.025.

[13] R. Sims, R. Schaeffer, B. Soares Moreira Cesar Borba, R. Schaeffer, F. Creutzig, X. Cruz-Núñez, D. Dimitriu, M.J. Figueroa Meza, L. Fulton, S. Kobayashi, O. Lah, A. McKinnon, P. Newman, M. Ouyang, J.J. Schauer, D. Sperling, G. Tiwari, Y. Sokona, E. Farahani, S. Kadner, K. Seyboth, A. Adler, I. Baum, S. Brunner, P. Eickemeier, B. Kriemann, J. Savolainen, S. Schlömer, C. von Stechow, T. Zwickel, J. Minx, Assessment Report 5: 8 Transport, (2014) 599–671. https://www.ipcc.ch/pdf/assessment-report/ar5/wg3/ipcc_wg3_ar5_chapter8.pdf.

[14] H. Tanaka, M. Uenishi, I. Tan, M. Kimura, J. Mizuki, An intelligent catalyst, (2001). http://papers.sae.org/2001-01-1301/.

[15] H. Tanaka, M. Taniguchi, N. Kajita, M. Uenishi, I. Tan, N. Sato, K. Narita, M. Kimura, Design of the Intelligent Catalyst for Japan ULEV Standard, Top. Catal.

30/31 (2004) 389–396. doi:10.1023/b:toca.0000029780.70319.36.

[16] M. Uenishi, M. Taniguchi, H. Tanaka, M. Kimura, Y. Nishihata, J. Mizuki, T. Kobayashi, Redox behavior of palladium at start-up in the Perovskite-type LaFePdO x automotive catalysts showing a self-regenerative function, Appl. Catal. B Environ. 57 (2005) 267–273. doi:10.1016/j.apcatb.2004.11.011.

[17] S. Solution, P. Particles, P. Metals, G. Growth, F.G. Growth, Self-regeneration of a Pd -perovskite Catalyst : A Philosopher's Stone for Today's Automotive Engine, Environ. Sci. (n.d.) 75–77.

[18] B. Saruhan, G.C. Mondragón Rodríguez, A.A. Haidry, A. Yüce, S. Heikens, W. Grünert, Integrated performance monitoring of three-way catalytic converters by self-regenerative and adaptive high-temperature catalyst and sensors, Adv. Eng. Mater. 18 (2016) 728–738. doi:10.1002/adem.201500410.

[19] Y. Farhang, E. Taheri-Nassaj, M. Rezaei, Pd doped LaSrCuO4 perovskite nano-catalysts synthesized by a novel solid state method for CO oxidation and Methane combustion, Ceram. Int. 44 (2018) 21499–21506. doi:10.1016/j.ceramint.2018.08.211.

[20] B. Kucharczyk, Catalytic Oxidation of Carbon Monoxide on Pd-Containing LaMnO3 Perovskites, Catal. Letters. 145 (2015) 1237–1245. doi:10.1007/s10562-015-1518-3.

[21] U.G. Singh, J. Li, J.W. Bennett, A.M. Rappe, R. Seshadri, S.L. Scott, A Pd-doped perovskite catalyst, BaCe1-x PdxO3-d, for CO oxidation, J. Catal. 249 (2007) 349–358. doi:10.1016/j.jcat.2007.04.023.

[22] Q. Zheng, M. Lail, K. Amato, J.T. Ennis, Pd doped CaCoxZr1-xO3-Δ perovskites for automotive emissions control, Catal. Today. 320 (2019) 30–39. doi:10.1016/j.cattod.2017.11.007.

[23] S.B. Varandili, A. Babaei, A. Ataie, A.A. Khodadadi, H. Kazerooni, Nano-structured Pd doped LaFe(Co)O3 perovskite; synthesis, characterization and catalytic behavior,

Mater. Chem. Phys. 205 (2018) 228–239. doi:10.1016/j.matchemphys.2017.11.030.

[24] I. Rossetti, O. Buchneva, C. Biffi, R. Rizza, Effect of sulphur poisoning on perovskite catalysts prepared by flame-pyrolysis, Appl. Catal. B Environ. 89 (2009) 383–390. doi:10.1016/j.apcatb.2008.12.017.

[25] E. Tzimpilis, N. Moschoudis, M. Stoukides, P. Bekiaroglou, Ageing and SO2 resistance of Pd containing perovskite-type oxides, Appl. Catal. B Environ. 87 (2009) 9–17. doi:10.1016/j.apcatb.2008.08.020.

[26] N.I. Mahyon, T. Li, R. Martinez-Botas, Z. Wu, K. Li, A new hollow fibre catalytic converter design for sustainable automotive emissions control, Catal. Commun. 120 (2019) 86–90. doi:10.1016/j.catcom.2018.12.001.

[27] G.C.M. Rodríguez, K. Kelm, S. Heikens, W. Grünert, B. Saruhan, Pd-integrated perovskites for TWC applications: Synthesis, microstructure and N 2O-selectivity, Catal. Today. 184 (2012) 184–191. doi:10.1016/j.cattod.2011.12.026.

[28] G.C. Mondragón Rodríguez, B. Saruhan, O. Petrova, W. Grünert, Pd-integrated perovskite as effective catalyst for selective catalytic reduction of NOx by propene, Top. Catal. 52 (2009) 1723–1727. doi:10.1007/s11244-009-9326-x.

[29] E. Tzimpilis, N. Moschoudis, M. Stoukides, P. Bekiaroglou, Preparation, active phase composition and Pd content of perovskite-type oxides, Appl. Catal. B Environ. 84 (2008) 607–615. doi:10.1016/j.apcatb.2008.05.016.

[30] S.A. Malamis, R.J. Harrington, M.B. Katz, D.S. Koerschner, S. Zhang, Y. Cheng, L. Xu, H.W. Jen, R.W. McCabe, G.W. Graham, X. Pan, Comparison of precious metal doped and impregnated perovskite oxides for TWC application, Catal. Today. 258 (2015) 535–542. doi:10.1016/j.cattod.2014.11.028.

[31] J.A. Onrubia-Calvo, B. Pereda-Ayo, A. Bermejo-López, A. Caravaca, P. Vernoux, J.R. González-Velasco, Pd-doped or Pd impregnated 30% La0.7Sr0.3CoO3/Al2O3

catalysts for NOx storage and reduction, Appl. Catal. B Environ. 259 (2019) 118052. doi:10.1016/j.apcatb.2019.118052.

[32] E.S.P.B. V, H. Schaper, L.L.V.A.N. Reijen, P. Chemistry, Gamma To Alpha Alumina.Pdf, 77 (1984) 383–393.

[33] V.A. Sadykov, L.A. Isupova, S.F. Tikhov, O.N. Kimkhai, Perovskite Catalysts: High-Surface Area Powders Synthesis, Monoliths Shaping and High-Temperature Applications, ChemInform. 26 (2010) no-no. doi:10.1002/chin.199550238.

[34] S. Keav, S. Matam, D. Ferri, A. Weidenkaff, Structured Perovskite-Based Catalysts and Their Application as Three-Way Catalytic Converters—A Review, Catalysts. 4 (2014) 226–255. doi:10.3390/catal4030226.

[35] B.F.K. Kingsbury, K. Li, A morphological study of ceramic hollow fibre membranes, J. Memb. Sci. 328 (2009) 134–140. doi:10.1016/j.memsci.2008.11.050.

[36] F.R. García-García, M.A. Rahman, B.F.K. Kingsbury, K. Li, Asymmetric ceramic hollow fibres: New micro-supports for gas-phase catalytic reactions, Appl. Catal. A Gen. 393 (2011) 71–77. doi:10.1016/j.apcata.2010.11.028.

[37] A. Christoffel, N. Preller, Numerical modelling of flow through packed beds of uniform spheres, (2011).

[38] W. Yang, R. Zhang, B. Chen, N. Bion, D. Duprez, S. Royer, Activity of perovskite-type mixed oxides for the low-temperature CO oxidation: Evidence of oxygen species participation from the solid, J. Catal. 295 (2012) 45–58. doi:10.1016/j.jcat.2012.07.022.

[39] N. Russo, P. Palmisano, D. Fino, Pd substitution effects on perovskite catalyst activity for methane emission control, Chem. Eng. J. 154 (2009) 137–141. doi:10.1016/j.cej.2009.05.015.

[40] R. Zhang, H. Alamdari, S. Kaliaguine, Fe-based perovskites substituted by copper and

palladium for NO + CO reaction, 242 (2006) 241–253. doi:10.1016/j.jcat.2006.05.033.

Highlights

- Pd-doped perovskite catalysts efficient for catalytic converter.
- Integration of perovskite catalyst into micro-structured ceramic hollow fibre without additional washcoating materials.
- Greater catalyst utilisation at low precious metal content.
- Excessive catalyst deposition created high mass transfer resistance.

List of Tables

546 **Table 1**

547

Catalyst	Catalyst amount (mg)	Reactor configuration	T_{50} (ºC)	Reference
LaFe	75	Packed-bed	270	[38]
$LaFe_{0.94}Pd_{0.06}O_3$			240	
$LaFe_{0.74}Cu_{0.2}Pd_{0.06}O_3$			240	
$LaSrCuO_4$	250	Packed-bed	220	[19]
$LaSrCu_{0.9}Pd_{0.1}O_4$			200	
$LaFe_{0.6}Co_{0.4}O_3$	100	Packed-bed	285	[23]
$LaFe_{0.57}Co_{0.38}Pd_{0.05}O3$			142	
$LaFeO_3$	100	Packed-bed	535	[39]
$LaFe_{0.9}Pd_{0.1}O_3$			495	
$LaMnO_3$			485	
$LaMn_{0.9}Pd_{0.1}O_3$			425	
$LaFeO_3$	100	Packed-bed	330	[40]
$LaFe_{0.97}Pd_{0.03}O_3$			230	
$LaFeO_3$	100	Packed-bed	249	[12]
$LaFePd_{0.05}O_3$			150	
$LaMnO_3$			249	
$LaFePd_{0.05}O_3$			170	
$LaCoO_3$			190	
$LaCoPd_{0.05}O_3$			155	

548

549 **Table 2**

550

Sample	S_{BET} (m^2g^{-1})	Average Crystallite Size (nm)	XRD Crystal Structure
$LaFe_{0.7}Mn_{0.225}Pd_{0.075}O_3$	20.69 ± 0.09	24.01	Orthorhombic
$LaFe_{0.7}Co_{0.225}Pd_{0.075}O_3$	10.73 ± 0.05	27.88	Orthorhombic
Alumina Hollow Fibre Substrate	1.42 ± 0.01	-	-
5mg 0.075 Pd/ γ-Al_2O_3 hollow fibre composite, Calcination at 500 ^oC	4.55 ± 0.01	-	-
5mg 0.075 Pd/ γ-Al_2O_3 hollow fibre composite, Calcination at 700 ^oC	3.99 ± 0.01	-	-

551

552 **Table 3**

553

Catalyst	Condition	T_{50} (°C)
$LaFe_{0.7}Mn_{0.225}Pd_{0.075}O_3$	5 mg	242
$LaFe_{0.7}Mn_{0.225}Pd_{0.075}O_3$	10 mg	213
$LaFe_{0.7}Co_{0.225}Pd_{0.075}O_3$	5 mg	252
$LaFe_{0.7}Co_{0.225}Pd_{0.075}O_3$	10 mg	235

554

555 **Table 4**

556

Catalyst	Condition	T_{50} (°C)
$LaFe_{0.7}Mn_{0.225}Pd_{0.075}O_3$	Packed-bed	242
$LaFe_{0.7}Mn_{0.225}Pd_{0.075}O_3$	Hollow Fibre	232
$LaFe_{0.7}Co_{0.225}Pd_{0.075}O_3$	Packed-bed	252
$LaFe_{0.7}Co_{0.225}Pd_{0.075}O_3$	Hollow Fibre	248

557

558

559 **Table 5**

560

Catalyst	Condition	T_{50} (ºC)
$LaFe_{0.7}Mn_{0.225}Pd_{0.075}O_3$	Packed-bed	215
$LaFe_{0.7}Mn_{0.225}Pd_{0.075}O_3$	Hollow Fibre	222
$LaFe_{0.7}Co_{0.225}Pd_{0.075}O_3$	Packed-bed	237
$LaFe_{0.7}Co_{0.225}Pd_{0.075}O_3$	Hollow Fibre	245

561

562

List of Figures

587

588 **Figure 1**

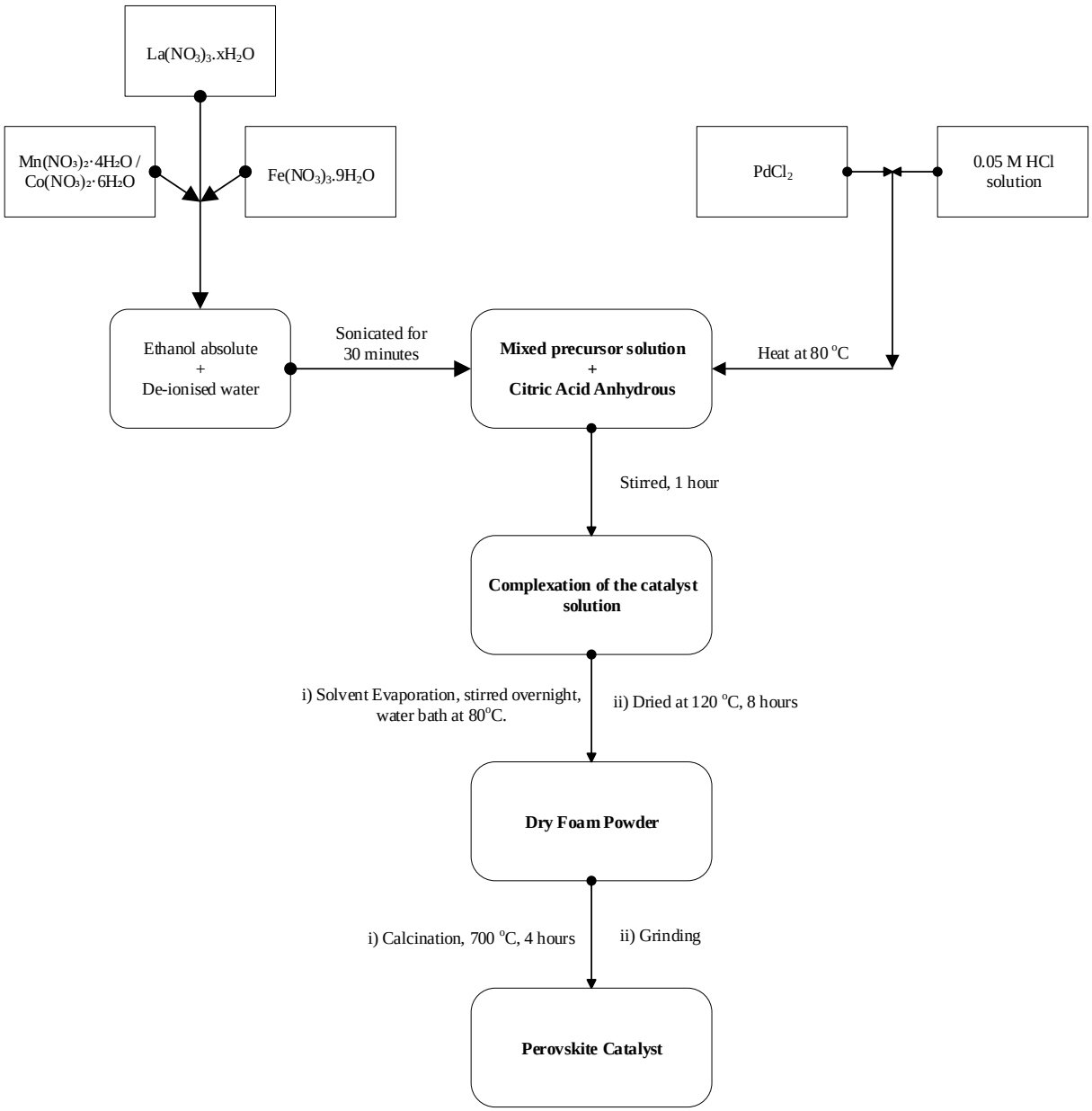

589

590

Figure 2

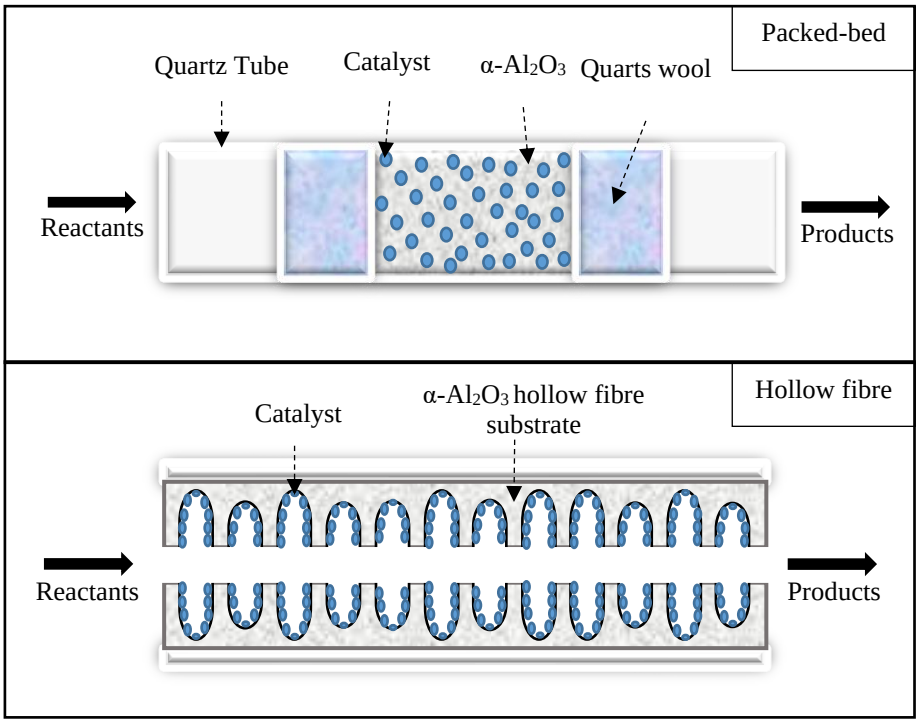
Packed-bed
Quartz Tube
Catalyst
α-Al2O3
Quarts wool
Reactants
Products
Hollow fibre
Catalyst
α-Al2O3 hollow fibre substrate
Reactants
Products

614 **Figure 3**

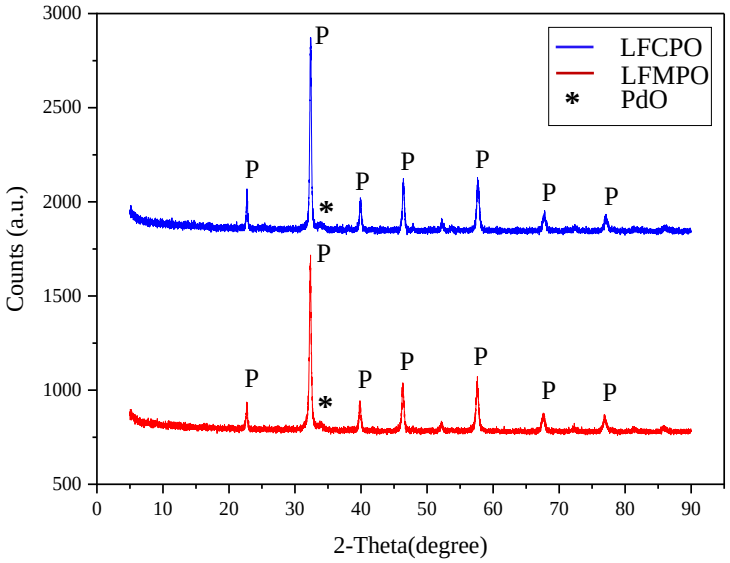

615

616

617

618

619

620

Figure 4

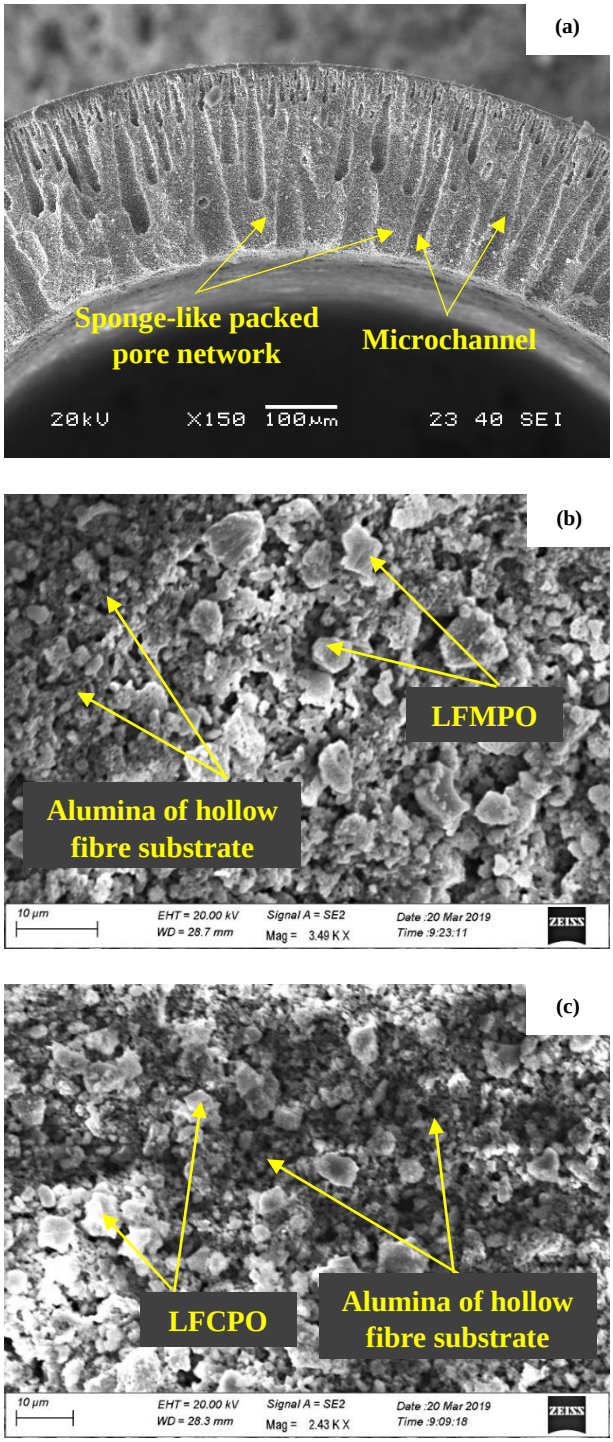

621

622

623

624

Figure 5

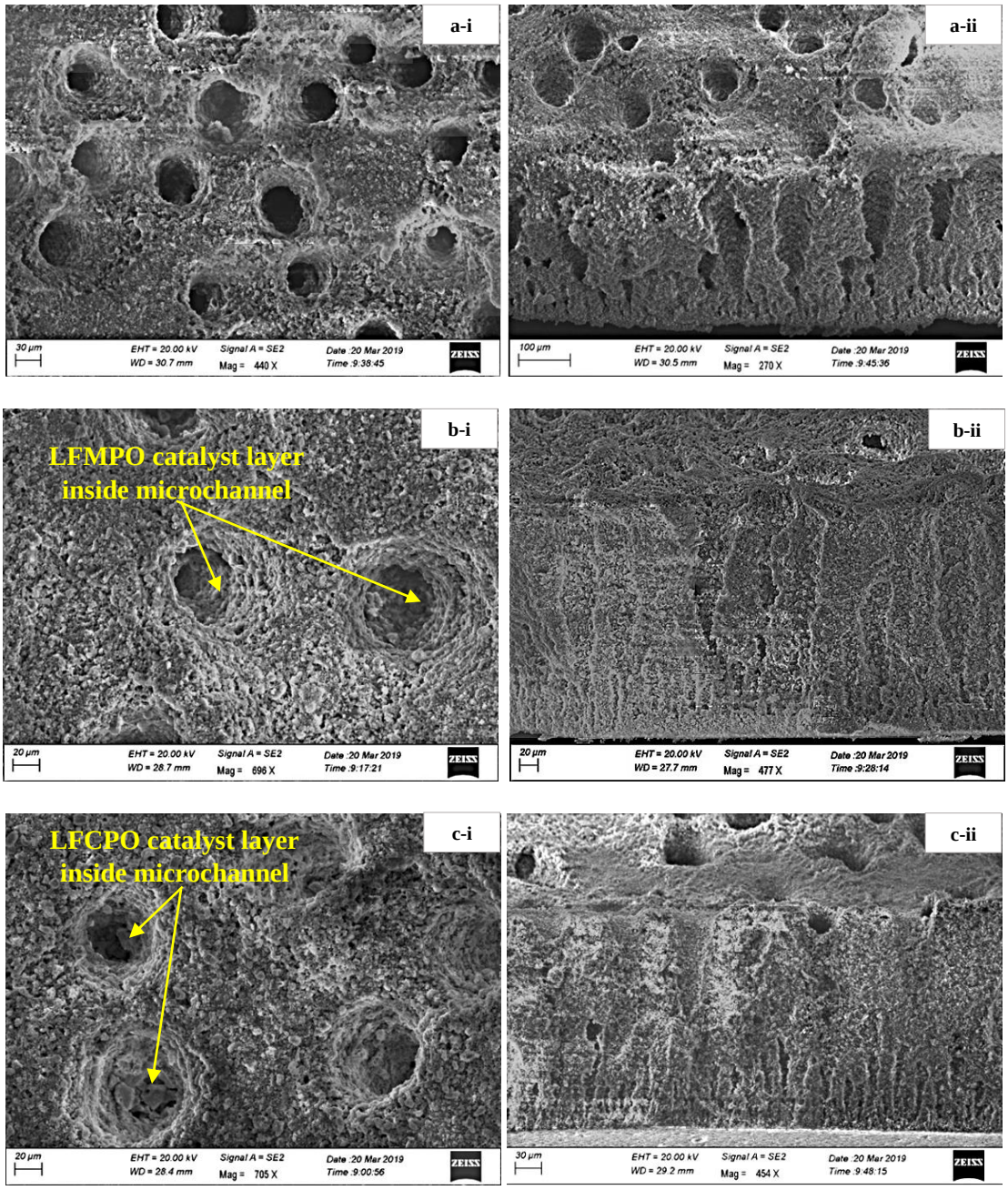

625

626

627

628 **Figure 6**

629

630

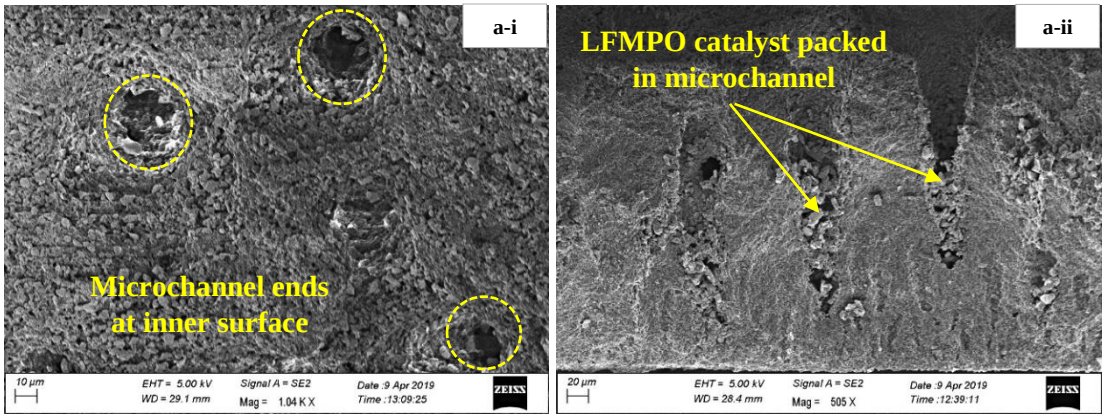

631

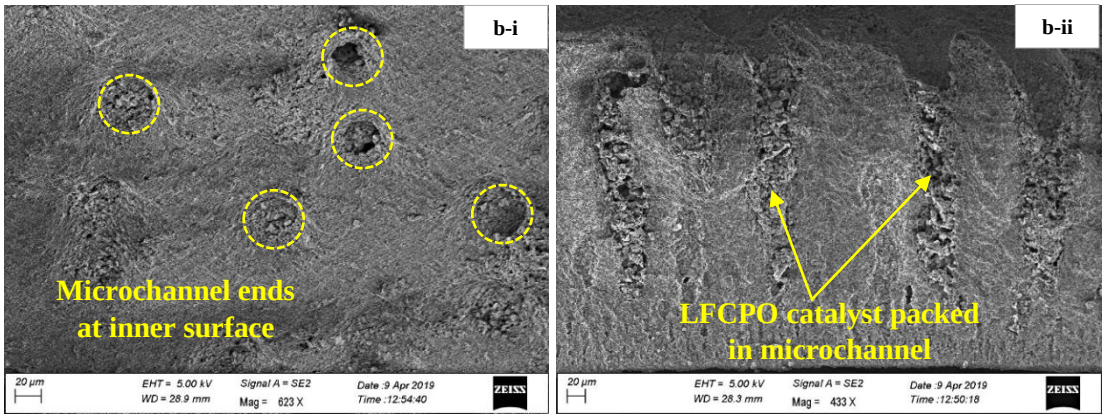

632

633 **Figure 7**

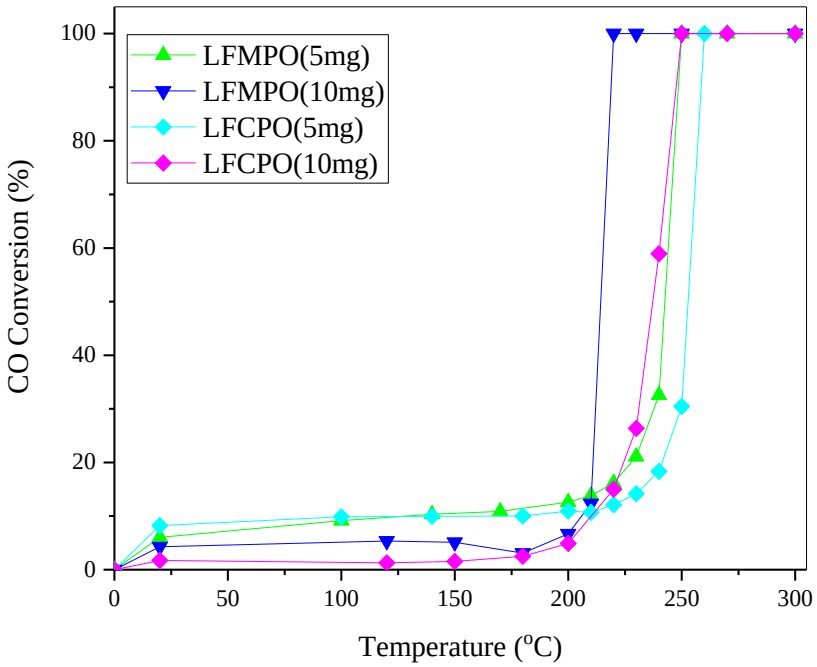

634

635

636

637

638

639

640

641

642

643

644

645

646

647

Figure 8

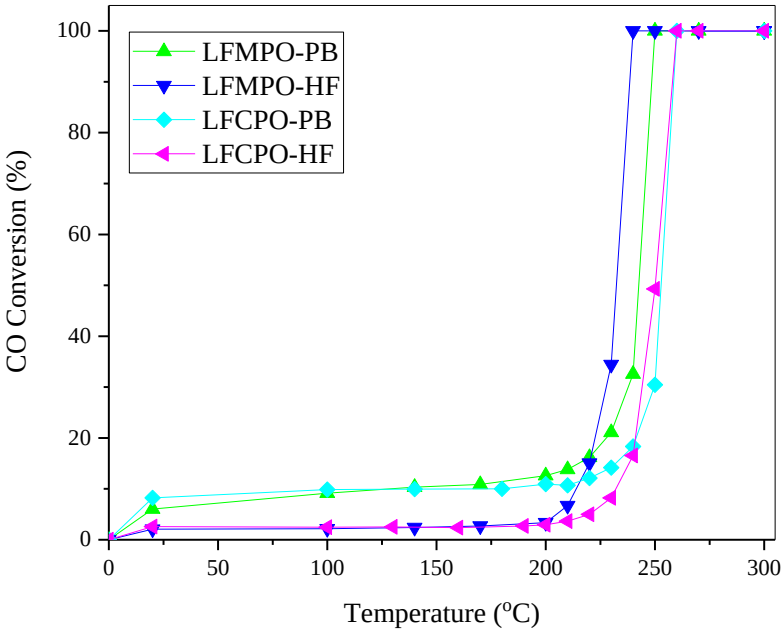
LFMPO-PB
LFMPO-HF
LFCPO-PB
LFCPO-HF
CO Conversion (%)
Temperature (°C)
0
20
40
60
80
100
0
50
100
150
200
250
300

Figure 9

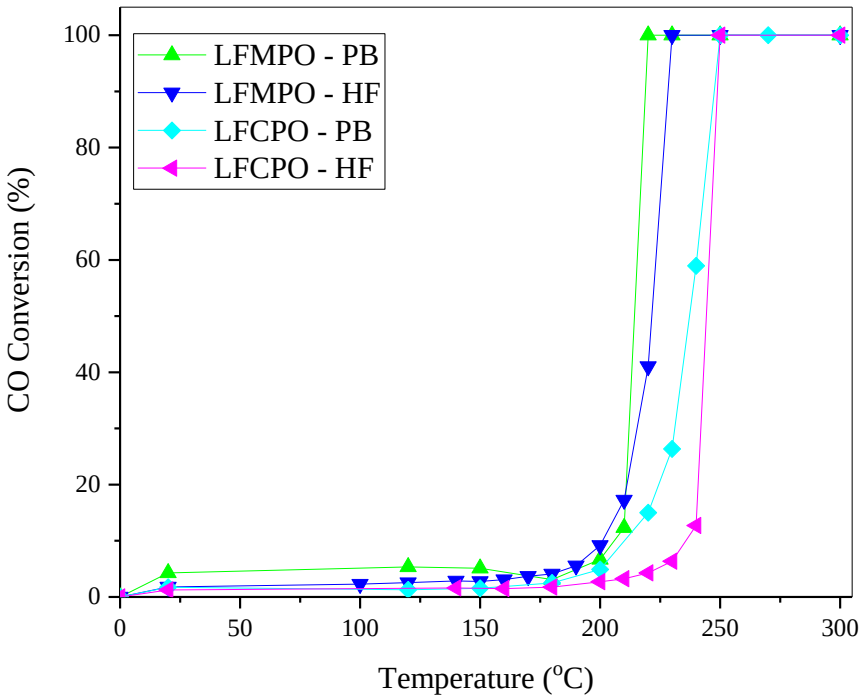
LFMPO - PB
LFMPO - HF
LFCPO - PB
LFCPO - HF
CO Conversion (%)
Temperature (°C)
0
20
40
60
80
100
0
50
100
150
200
250
300

681

682 **Figure 10**

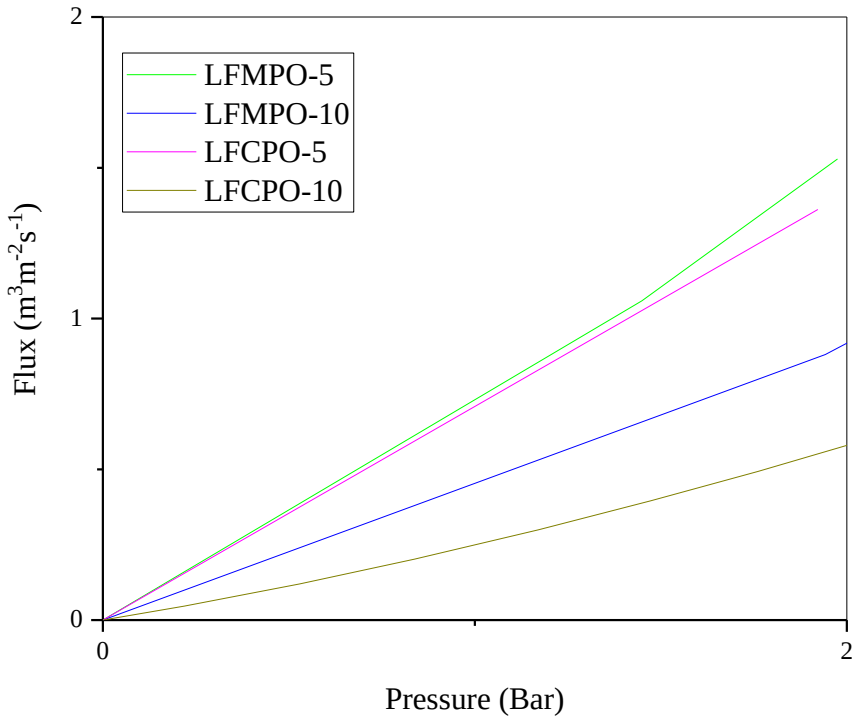

683